Predictive Energy-Efficient Driving Strategy Design of Connected Electric Vehicle among Multiple Signalized Intersections

Haoxuan Dong[a,1], Weichao Zhuang[a,1], Boli Chen[b], Yanbo Lu[a], Shuaipeng Liu[a], Liwei Xu[a], Dawei Pi[c], Guodong Yin[a,*]

[a] School of Mechanical Engineering, Southeast University, Nanjing 211189, China

[b] Department of Electronic and Electrical Engineering, University College London, London, UK

[c] School of Mechanical Engineering, Nanjing University of Science and Technology, Nanjing 210094, China

[*] Corresponding author, E-mail address: ygd@seu.edu.cn; Tel.: +86-13913879060

1 These authors contributed equally to this work

Abstract: Signalized intersections dominate traffic flow in urban areas, resulting in increased energy consumption and travel delay for the vehicles involved. To mitigate the negative effect of traffic lights on eco-driving control of electric vehicles, a multi-intersections-based eco-approach and departure strategy (M-EAD) is proposed to improve vehicle energy efficiency, traffic throughput, and battery life, while maintaining acceptable driving comfort. M-EAD is a two-stage control scheme that includes efficient green signal window planning and speed trajectory optimization. In the upper stage, the traffic light green signal window planning is formulated as a shortest path problem, which is solved using an A* algorithm for travel delay reduction. In the lower stage, the speed optimization problem is solved by resorting to a receding horizon framework, in which the energy consumption and battery life losses are minimized using an iterative dynamic programming algorithm. Finally, Monte Carlo simulation with randomized traffic signal parameters is conducted to evaluate the performance of the proposed M-EAD strategy. The results show the various advancements of the proposed M-EAD strategy over two benchmark methods, constant speed and isolated-intersection-based eco-approach and departure strategies in terms of energy efficiency, travel time, and battery life in stochastic traffic scenarios. In addition, the performance of M-EAD on actual road conditions is validated by on-road vehicle test.

Keywords: electric vehicle, connected vehicle, energy-efficient driving, speed planning, real-world vehicle experiment

Acronyms			
CAV	Connected and automated vehicle	I-EAD	Isolated-intersection-based EAD
CS	Constant speed	M-EAD	Multi-intersections-based EAD
DP	Dynamic programming	OCP	Optimal control problem
EAD	Eco-approach and departure	RHVO	Receding horizon velocity optimization
EVs	Electric vehicles	SPaT	Signal phase and timing
IDP	Iterative dynamic programming	V2I	Vehicle-to-infrastructure

1. Introduction

The increasing interest in environmental protection and resource conservation has prompted researchers to develop eco-friendly technologies to reduce vehicle energy consumption [1-3]. A promising method involves driving the vehicle at an appropriate speed, which is also called eco-driving control [4]. By operating vehicles at smooth speeds, eco-driving can reduce excessive energy consumption and greenhouse emissions, and even improve traffic throughput [5, 6]. Eco-driving is considered to have great commercialization potential in the near future [7].

The emerging connected and automated vehicle (CAVs) technology has redefined eco-driving. By utilizing the shared look-ahead traffic information, the CAVs can optimize their speed trajectory to improve vehicle operating efficiency [8-10]. Predictive cruise control, an eco-driving application for vehicles on highways, uses road geometry information, such

as road grades and curvatures, to develop a look-ahead cruising strategy with variable speeds [11, 12]. To execute predictive cruise in the real world, some studies have considered the influence of preceding vehicles [13]. Another typical application of eco-driving is eco-approach and departure (EAD) control at signalized intersections [14]. It principally involves avoiding stop-and-go behavior by optimizing the vehicle speed to improve the vehicle's energy efficiency. Different studies focus on the EAD strategy, which can be divided into isolated-intersection-based EAD (I-EAD) and multi-intersections-based EAD (M-EAD) strategies.

Most existing research on EAD control focuses on speed optimization at isolated signalized intersections. Katsaros *et al.* [15] developed a green light optimized speed advisory system for fuel consumption minimization by avoiding stopping at the red signal. Simulation results indicated that a higher EAD system penetration rate could future improve the energy efficiency of on-road vehicles. To enhance the eco-driving strategy in real traffic situations, Li *et al*. [16] proposed an energy-saving departure strategy for a connected vehicle at an intersection, which calculates the vehicle speed using the Legendre Pseudo Spectral algorithm and considers the constraints of the preceding vehicle. However, the speed profiles of the preceding vehicle are known as a priori, which is impractical. Ye *et al.* [17] developed an enhanced EAD strategy with speed forecasting of the preceding vehicle. Dong *et al*. [18] proposed a hierarchical eco-approach control algorithm that considers the vehicle queue at a signalized intersection. The vehicle arrives at the intersection stop line just as the last queued vehicle is discharged by predicting the movement of the vehicle queue. Zeng *et al.* [19] proposed a globally optimal speed planning strategy for a vehicle running on a given route with multiple stop signs, traffic lights, turns, and curved segments. After converting traffic light and road geometry to spatial-temporal constraints, the optimization problem was solved using dynamic programming (DP). Another study presented by Shao *et al*. [20, 21] proposed a fuel-efficient control framework that integrates speed optimization and traffic states (i.e., traffic flow speed and density) prediction. This control framework can be used in partially connected traffic scenarios and extended to multiple intersections or multi-lane scenarios in the future. In addition, Hao *et al.* [22] and Sun *et al.* [23] investigated the effect of actual traffic signals with uncertain signal phase and timing (SPaT) on eco-driving. A modified EAD strategy was proposed to for enhanced robustness. With the development of artificial intelligence, reinforcement learning has been utilized to design the EAD strategy, which demonstrates robust performance under complex driving conditions [24-26].

The I-EAD strategy has been shown effective in the context of a single intersection scenario. However, the performance of an I-EAD degrades when it is applied to multi-intersection conditions owing to the spatial-temporal correlation among multiple traffic signals. Accordingly, some recent studies have investigated EAD control among multiple intersections. Du *et al.* [27] and Chalaki *et al.* [28] developed a distributed eco-driving strategy for CAVs in multiple unsignalized intersections, which improved vehicle fuel efficiency and traffic throughput via vehicle speed planning. To enhance the eco-driving strategy in real traffic situations, Asadi *et al*. [29] utilized the preview information of traffic SPaT to design a rule-based EAD control strategy and proposed a speed tracking controller for collision avoidance with preceding vehicles. Dong *et al.* [30] considered spatial and temporal constraints from multiple signalized intersections and vehicle queues and proposed a two-level controller with energy-economy speed optimization and safe intervehicle distance for CAVs. Another EAD was proposed by Yang *et al.* [31], where a modular and scalable eco-driving system rapidly calculates a fuel-optimized speed while traversing more than one signalized intersection. To improve the multi-intersections EAD problem solving efficiency, Lin *et al.* [32, 33] extracted near-optimal operating rules from the results obtained by optimally solving a single intersection crossing problem. As such, the problem of multiple intersections is addressed by combining the two- or three-stage near-optimal operating rules. Nevertheless, only simulation tests were conducted; therefore, the performance of the proposed method in the real-world application is uncertain. Wu *et al.* [34] proposed a computationally efficient algorithm for EAD along signalized corridors with a hierarchal framework by combining target traffic signal cycle determination and optimal trajectory planning, and conducted a field implementation in a sheltered traffic environment. Although explicit vehicle dynamics and powertrain models are included, the study was optimized based on a parabolic speed trajectory, which may not be able to optimize vehicle speed. In addition, the

aforementioned multiple intersections EAD studies are all based on internal combustion engine vehicles (ICEVs). However, the future of road vehicle powertrains is electric, which could lead to drastically different eco-driving behavior due to different powertrain characteristics and control objectives, such as motor dynamics and battery health.

This paper proposes an M-EAD strategy for electric vehicles (EVs) with a two-stage control framework to optimize an aggregated cost involving energy efficiency, travel time, battery life degradation, and driving comfort. The major contributions of this study are threefold: First, we propose an optimal control problem (OCP) formulation for the multiple-intersection crossing of an EV with consideration of a comprehensive cost that accounts for vehicle energy efficiency, travel time, battery life, and driving comfort goals. Second, the formulated multi-objective OCP is addressed by a novel two-stage M-EAD strategy that incorporates an efficient green signal window planning stage and speed trajectory optimization stage to efficiently solve the OCP. The former is solved by an improved A* algorithm, while the latter is addressed by a receding horizon velocity optimization (RHVO) strategy based on an iterative dynamic programming (IDP) algorithm. Third, we conduct a Monte Carlo simulation case study to evaluate the robustness of the proposed M-EAD strategy under stochastic traffic conditions. In addition, a field experiment is conducted to validate the proposed method in real-world driving scenarios.

The remainder of this paper is organized as follows. Section 2 introduces the model of multi-intersections and vehicle dynamics. In Section 3, the OCP of EAD for multiple intersections driving is formulated, and the control framework of M-EAD is introduced. Sections 4 and 5 develop an efficient green signal window planning method and the RHVO strategy, respectively. The performance of the proposed method is evaluated by simulation and real-world vehicle experiments in Sections 6 and 7, respectively. Finally, Section 8 concludes the paper.

2. Multiple Signalized Intersections Model and Vehicle Dynamics

This section introduces the driving scenario of the connected EVs, which is to be driven along a predefined route with multiple signalized intersections. For brevity, we use "green window" to represent the green traffic signal interval in the rest of this paper. In addition, models of multiple intersections and vehicle dynamics are presented.

2.1 Multiple Signalized Intersections Model

We define a generic route, as shown in Fig. 1, with N_t signalized intersections as a set $\mathcal{R} = \{\mathcal{F}, \mathcal{S}\}$, where $\mathcal{F}$ is the frame of the route, and $\mathcal{S} = \{\mathcal{S}_k | k \in \mathcal{I}\}$ (where $\mathcal{I} = \{1, 2, \cdots, N_t\}$) is the set of all traffic signals. The subset $\mathcal{S}_k$ of the kth traffic light that collects its position, S^k, and SPaT information, is defined $\mathcal{S}_k = \{S^k, T_s^k, P^k, T_g^k, T_r^k, C^k\}$, where T_s^k is the initial indication of the transition time when the host vehicle approaches, C^k is the accumulated number of cycles of the traffic signal, and P^k is the initial indication of the traffic signal. Without loss of generality, let $P^k = 1$ denote the green signal and $P^k = 0$ denote the red signal. Finally, T_g^k and T_r^k are the intervals of the green and red signals (for safety purposes, the yellow signal is simply treated as a red one), respectively. The host vehicle is equipped with a vehicle-to-infrastructure (V2I) communication device (4G or LTE-V), thus the traffic information (i.e., route distance, traffic signal SPaT, and speed limits) can be accessed by communicating with Road Side Units or the Cloud.

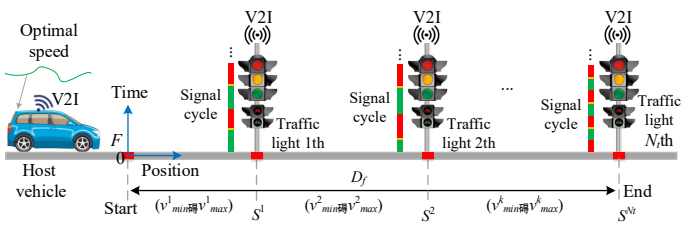

Fig. 1. The travel route with multiple signalized intersections.

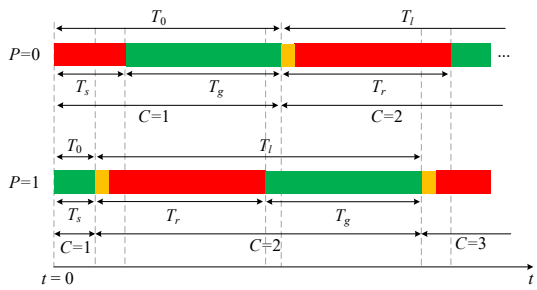

Fig. 2. Graphical representations of the traffic signal cycle. Each colored block represents a signal phase.

The road speed limit set is defined as $\mathbb{V}_{min} = [v_{min}^1, \cdots, v_{min}^{N_t}]$ and $\mathbb{V}_{max} = [v_{max}^1, \cdots, v_{max}^{N_t}]$, where v_{min}^k and v_{max}^k are the minimum and maximum speed limits for road segments between intersections, respectively. Let the total length of the route be D_f, then the position of the traffic signal $S^k \in [0, D_f]$, and the set $\mathbb{S}_t = [S^1, \cdots, S^{N_t}]$.The distances between two traffic signals S^k and S^{k-1} is defined as D^k as Eq. (1).

$$D^k = \begin{cases} S^k & if\ k = 1 \\ S^k - S^{k-1} & if\ k > 1 \end{cases} \tag{1}$$

In general, a traffic signal is operated with an independent signal-clock period. Fig. 2 shows a graphical representation of a typical signal cycle for a through-movement lane. To simplify counting the signal states, it is assumed that a full signal cycle starts with the beginning of the red (or yellow) light and ends with the ends of the green light. As such, the initial signal cycle length T_0^k and the standard signal cycle length T_l^k are defined by Eqs. (2) and (3), respectively with two typical examples illustrated in Fig. 2.

$$T_0^k = \begin{cases} T_s^k + T_g^k & P^k = 0, \\ T_s^k & P^k = 1. \end{cases} \tag{2}$$

$$T_l^k = T_g^k + T_r^k \tag{3}$$

With the initial signal cycle length, the accumulated number of cycles C^k of traffic signal S_k at any moment t, can be calculated using Eq. (4).

$$C^k = \text{ceil}\left(\frac{t - T_0^k}{T_l^k}\right) + 1 \tag{4}$$

where $\text{ceil}(u)$ yields the least integer greater than or equal to u. Finally, the starting times of the green and red signals for the C^kth cycle are defined as t_{g,C^k}^k and t_{r,C^k}^k respectively, as shown in Eqs. (5) and (6)

$$t_{g,C^k}^k = \begin{cases} \begin{cases} 0 & C^k = 1 \text{ and } P^k = 1 \\ T_s^k + T_r^k(C^k - 1) + T_g^k(C^k - 2) & C^k > 1 \text{ and } P^k = 1 \end{cases} \\ \begin{cases} T_s^k & C^k = 1 \text{ and } P^k = 0 \\ T_s^k + T_r^k(C^k - 1) + T_g^k(C^k - 1) & C^k > 1 \text{ and } P^k = 0 \end{cases} \end{cases} \tag{5}$$

$$t_{r,C^k}^k = \begin{cases} \begin{cases} \text{N/A} & C^k = 1 \text{ and } P^k = 1 \\ T_s^k + T_r^k(C^k - 2) + T_g^k(C^k - 2) & C^k > 1 \text{ and } P^k = 1 \end{cases} \\ \begin{cases} 0 & C^k = 1 \text{ and } P^k = 0 \\ T_s^k + T_r^k(C^k - 2) + T_g^k(C^k - 1) & C^k > 1 \text{ and } P^k = 0 \end{cases} \end{cases} \tag{6}$$

2.2 Vehicle Dynamics

2.1.1 Vehicle longitudinal dynamics

Since this paper investigates the daily driving scenario, the vehicle is driven with a reasonable margin to the limit of tire adhesion. Thus, tire slip is not considered and only the longitudinal dynamics are formulated as Eqs. (7) and (8).

$$\dot{d} = v \tag{7}$$

$$\dot{v} = \frac{F_v - (mgf\cos\theta + mg\sin\theta + 0.5C_D A\rho v^2)}{m\delta} \tag{8}$$

where d and v are the position and velocity of the vehicle, respectively. F_v is the vehicle force, that is, positive for propulsion and negative for braking. m is the mass of the vehicle, δ is the vehicle rotational inertia coefficient, g is the acceleration due to gravity, f is the rolling resistance coefficient, C_D is the aerodynamic drag coefficient, A is the vehicle frontal area, ρ is the air density, and θ is the road gradient.

For EVs, the vehicle force is supplied by the electric motor during propulsion and the vehicle braking force includes the motor generation and friction braking forces. Thus, the vehicle force is expressed by Eq. (9).

$$F_v = \begin{cases} F_m i_t \eta_t & \text{Propulsion} \\ \dfrac{F_m i_t}{\eta_t} + F_{bf} & \text{Braking} \end{cases} \tag{9}$$

where F_m is the desired motor force, F_{bf} is the friction braking force, i_t is the transmission ratio including the gearbox and final drive, and η_t is the driveline efficiency. The wheel force of the EVs is affected by the propulsion and braking torque allocation strategies. In this study, the propulsion force of each wheel in the front axle was equally allocated, and the regenerative braking strategy proposed in [35] was used.

2.1.2 Quasi-static Motor Model

Consider η_m the motor working efficiency, which is depicted in Fig. 3 as a look-up table. The quasi-static model was used to calculate the energy loss of the motor, as shown in Eq. (10).

$$P_{m\_loss} = P_m \cdot \left(\eta_m{}^{-\mathrm{sign}(P_m)} - 1\right) \cdot \mathrm{sign}(P_m) \tag{10}$$

where sign( ) is the signum function, P_{m_loss} is the motor power loss. P_m is the required motor power, positive for propulsion and negative for generation, as given in Eq. (11)

$$P_m = \frac{F_m r_w \omega}{9.55} = \frac{F_m r_w}{9.55} \cdot 60 \frac{v}{2\pi r_w} i_g i_0 \tag{11}$$

where r_w the wheel radius and ω the motor rotational speed.

2.1.3 Battery Model

The battery provides electricity when the vehicle is in traction, and recovers energy when the vehicle is in the regenerative braking mode. The required instantaneous battery power P_b was calculated using Eq. (12).

$$P_b = P_m + P_{m\_loss}\mathrm{sign}(P_{m\_loss}) + P_a \tag{12}$$

where P_a is the accessory power. We used a simplified equivalent circuit model to represent the dynamics of the battery [36]. The changing rate of battery state of charge (SOC) was calculated using Eq. (13).

$$S\dot{O}C = -\frac{V_{oc} - \sqrt{V_{oc}^2 - 4P_b R_b}}{2Q_b R_b} \tag{13}$$

where V_{oc} is the open-circuit voltage, R_b is the internal resistance, Q_b is the maximum capacity of the battery. The relationships of V_{oc} and R_b, with respective to SOC, respectively, are displayed in Figs. 4 and 5, which were obtained from the experimental results. The battery power loss P_{b_loss} was calculated using Eq. (14).

$$P_{b\_loss} = {I_b}^2 R_b \tag{14}$$

where I_b is the battery current, which is expressed as $I_b = P_b/(V_{oc} - I_b R_b)$. In addition, the state of health model for the battery considers the battery life during vehicle speed optimization. Because the discharge/charge rate and depth of discharge are identified as the main factors leading to battery aging, a widely used semi-empirical model is adopted here to calculate the battery capacity loss Q_{loss} [37], as described in Eq. (15)

$$Q_{loss} = B(I_c) \cdot \exp\left(\frac{-E_a(I_c)}{RT_\mathrm{b}}\right)(A_h)^z \tag{15}$$

where I_c is the instantaneous battery discharge/charge rate, T_b is the absolute temperature of the battery, R is the ideal gas constant, and z is the exponential factor. $B(I_c)$ is the impact factor determined by I_c, as shown in Fig. 6, where the relationship is obtained by fitting experimental data. $E_a(I_c)$ is the activation energy, which was calculated by $E_a = 31700 - 370.3I_c$. A_h is the discharge/charge Ah-through-flow, determined by $A_h = \int I_b \, \mathrm{d}t/3600$.

3. Problem Formulation and Control Framework

This section introduces the OCP of EAD control, which aims to simultaneously minimize the energy consumption and travel time required to drive through multiple signalized intersections. Then, the framework of the M-EAD strategy that addresses the OCP is formulated.

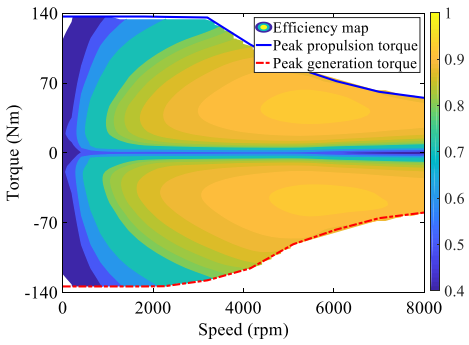

Fig. 3. Map of motor working efficiency.

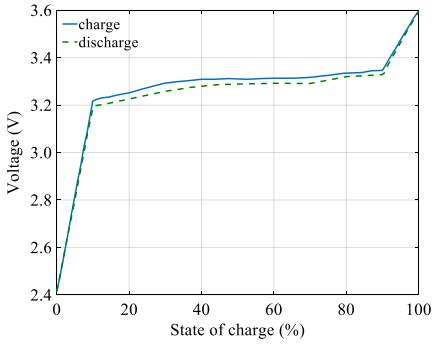

Fig. 4. Open circuit voltage of battery cell.

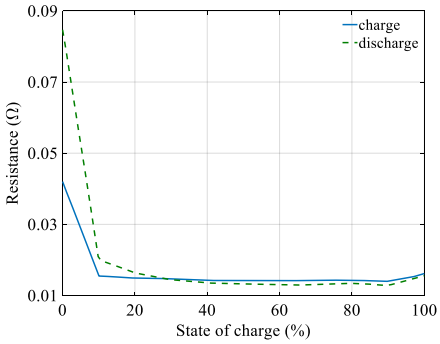

Fig. 5. Inner resistance of battery cell.

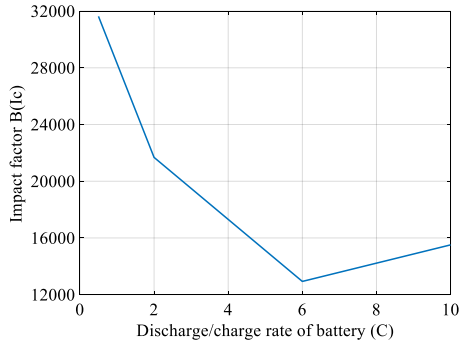

Fig. 6. Correlation of the impact factor and discharge rate.

3.1 Problem Formulation

Two common strategies for a vehicle driving through route $\mathcal{R}$ are defined in Section 2.1: the constant speed (CS) and I-EAD strategies. Fig. 7 shows the possible position profiles of CS, I-EAD, and M-EAD strategies while passing through a route with multiple intersections.

The CS strategy emulates a traditional human-driven vehicle, which tends to drive at a constant speed and to decelerate to a stop at a constant rate when facing a red traffic light. When the traffic light switches to green, the vehicle applies a constant acceleration until it reaches the desired constant speed [38]. The blue dashed line in Fig. 7 represents a typical case of the CS strategy. The vehicle has to stop for the second and third traffic signals, which leads to increased vehicle energy consumption and travel delay due to inefficient stop-and-go operations.

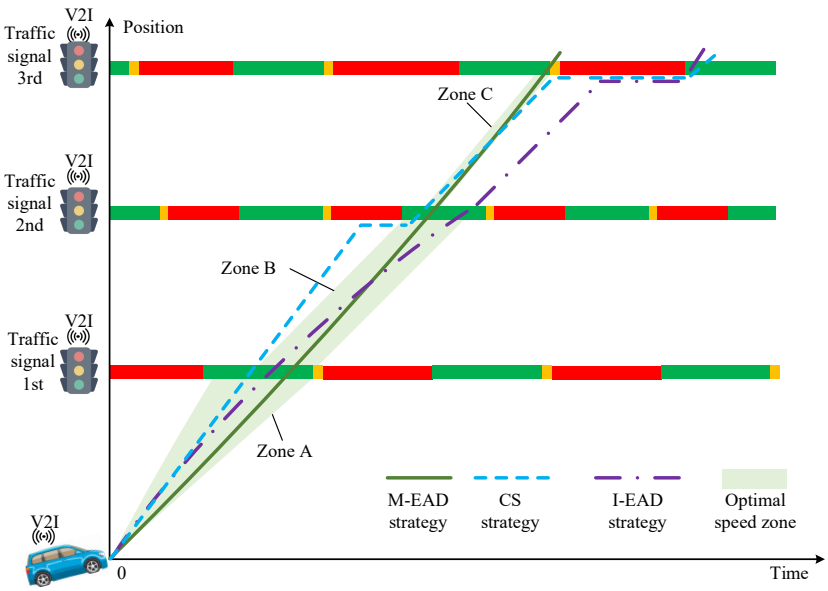

Fig. 7. Position profiles of vehicles passing through three consecutive intersections.

The I-EAD is the most common eco-driving strategy for multiple intersections crossing scenarios, which divides the multi-intersections driving problem into single intersection crossing problems and successively optimizes the vehicle speed profile for efficiently driving through each intersection in order. The I-EAD is designed from a local perspective (for an isolated intersection) while ignoring the spatial relationship of traffic light positions and the temporal relationship of traffic light SPaT, therefore its control solution could still yield suboptimal solutions in multiple-intersection scenarios. The dashed-dotted trajectory in Fig. 7 shows a typical solution of the I-EAD. As it can be seen, the strategy can avoid the stop-and-go operation at the first and second signalized intersections; however, the vehicle has to stop for the third intersection, which incurs a delay.

Therefore, this study uses the information of multiple intersections to optimize the vehicle speed profile for the entire mission, as indicated by the green solid line in Fig. 7. The OCP of multi-intersections eco-driving control is formulated as shown in Eqs. (16) and (17), where the objective is designed to reduce energy losses, travel time, and battery degradation while maintaining acceptable driving comfort

$$\underset{\boldsymbol{u}\in \boldsymbol{U}}{\text{Minimize}} \quad J(u,x) = \int_0^{T_p} \{\alpha_1 (P_{m\_loss} + P_{b\_loss}) + \alpha_2 |\dot{a}| + \alpha_3 Q_{loss}\} dt + \alpha_4 T_p \tag{16}$$

s.t

$$\dot{x} = f(x,u) \tag{17a}$$

$$x(0) = [0, v_s]^T,\ d(T_p) = D_f \tag{17b}$$

$$v_{min} \le v \le v_{max} \tag{17c}$$

$$u_{min} \le u \le u_{max} \tag{17d}$$

$$\begin{aligned} x = [S^k, 0]^T \quad if\ d = S^k \text{ and } t \in \left(t_{r,C^k}^k, t_{r,C^k}^k + T_r^k\right), \forall k \\ x = [S^k, v]^T \quad if\ d = S^k \text{ and } t \in \left(t_{g,C^k}^k, t_{g,C^k}^k + T_g^k\right), \forall k \end{aligned} \tag{17e}$$

where $x = [d, v]^T$ is the state vector, $u = F_v$ is the control input, and the different equation Eq. (17a) follows the vehicle longitudinal dynamics given in Eqs. (7)-(8). T_p is the travel time for the entire trip. $u_{min} < 0$ and $u_{max} \ge 0$ are the maximum braking and propulsion forces, respectively.

In Eq. (16), the first term improves the vehicle energy efficiency by minimizing the vehicle energy losses, that is, motor and battery loss. The second term reduces the increment in acceleration/deceleration for smooth speed change, which is related to the driving comfort. The third term minimizes the battery capacity loss during operation to prolong the battery life. To improve overall traffic throughput, travel time is also minimized. α_1, α_2, α_3, and α_4 are the weighing factors for the four objectives. Several constraints are defined in Eq. (17) to satisfy the system differential equation (Eq. (17a)), the initial and terminal states (Eq. (17b)), speed limits (Eq. (17c)), physical operation bounds (Eq. (17d)), and intersection requirements (Eq. (17e)).

3.2 Control Framework

The formulated OCP is a highly non-convex optimization problem, it is difficult to directly calculate the optimal control rule or vehicle speed trajectory because of the nonlinear objectives (battery and motor losses and battery capacity loss), and a variety of constraints (such as initial and terminal boundary constraints, states constraint, control constraint, and mixed constraint). Thus, this paper proposes a hierarchical control scheme, namely, the M-EAD strategy, as depicted in Fig. 8. The M-EAD strategy is composed of two stages: efficient green window planning and vehicle speed optimization. In the upper stage, the travel time is minimized by planning the green window of each intersection for mobility efficiency. The formulated travel time minimization problem was solved using an A* shortest path algorithm. In the lower stage, an RHVO strategy is proposed based on the IDP to find the speed trajectory that simultaneously optimizes the energy efficiency, battery life, and driving comfort.

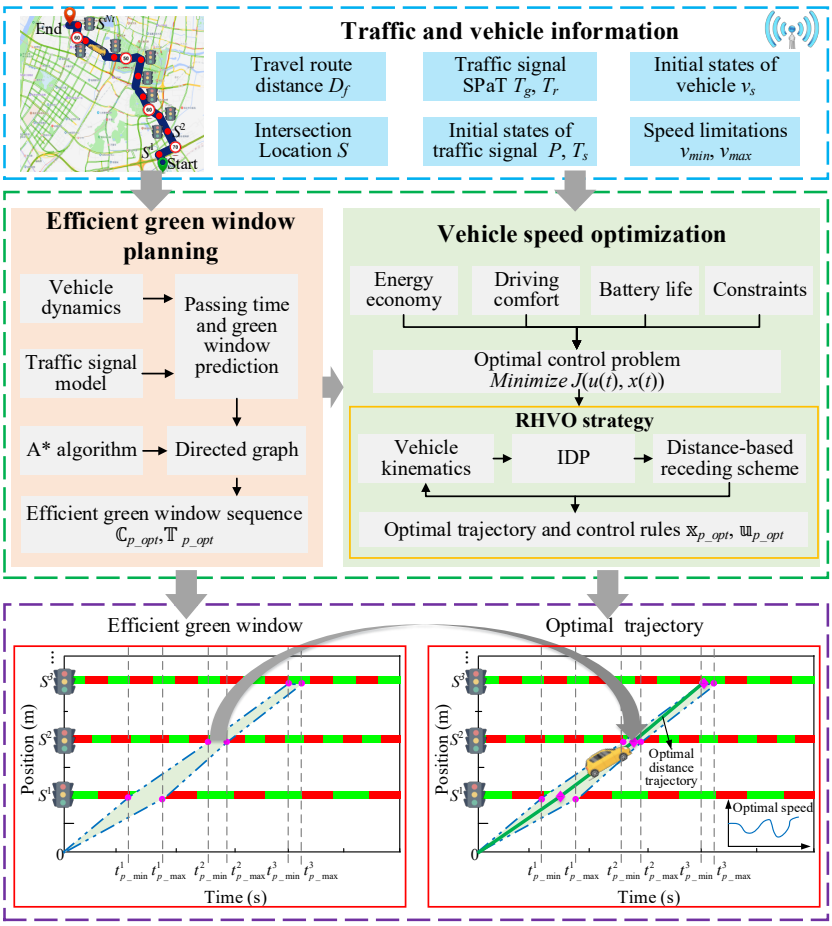

Fig. 8. The control scheme of the proposed M-EAD strategy.

4. Efficient Green Window Planning

To solve the energy-optimal problem for driving through a group of signalized intersections efficiently, the upper stage of M-EAD calculates a series of green windows for each intersection. The problem of green window planning is first described as a directed graph, and then solved using the shortest path method, that is, the A* algorithm. The derived green windows are imposed as constraints in the lower stage to optimize the speed profiles.

4.1 Green Window Planning Problem

First, we define a set $\mathbb{C}^k$ as a collection of feasible green windows for traffic signal $\mathcal{S}_k$ that the vehicle can reach subject to maximum and minimum speed limits. The set $\mathbb{C}^k$ is determined by the set of feasible kth intersection passing intervals $\mathbb{t}_p^k$, traffic SPaT information, vehicle initial states, and road speed limits. Assuming that the vehicle acceleration is constant for the feasible passing interval calculation, we can use Eqs. (18) and (19) to predict the passing time at intersection $\mathcal{S}_k$.

$$t_{p\_min}^k = \begin{cases} \text{ceil}\left(\dfrac{v_{max}^k - v_{avg}}{a_d} + \dfrac{D^k - \dfrac{(v_{max}^k)^2 - v_{avg}^2}{2a_d}}{v_{max}}\right) & if\ D^k > \dfrac{(v_{max}^k)^2 - v_{avg}^2}{2a_d} \\ \text{ceil}\left(\dfrac{-v_{avg} + \sqrt{v_{avg}^2 + 2a_d D^k}}{a_d}\right) & if\ D^k \le \dfrac{(v_{max}^k)^2 - v_{avg}^2}{2a_d} \end{cases} \tag{18}$$

$$t_{p\_max}^{k} = \begin{cases} \text{ceil}\left(\dfrac{v_{min}^{k} - v_{avg}}{a_b} + \dfrac{D^k - \dfrac{\left(v_{min}^{k}\right)^2 - v_{avg}^2}{2a_b}}{v_{max}}\right) & if\ D^k > \dfrac{\left(v_{min}^{k}\right)^2 - v_{avg}^2}{2a_b} \\ \text{ceil}\left(\dfrac{-v_{avg} - \sqrt{v_{avg}^2 + 2a_b D^k}}{a_b}\right) & if\ D^k \le \dfrac{\left(v_{min}^{k}\right)^2 - v_{avg}^2}{2a_b} \end{cases} \tag{19}$$

where $t_{p\_min}^{k} \in \mathbb{N}^+$ and $t_{p\_max}^{k} \in \mathbb{N}^+$ are the minimum and maximum passing times, respectively. v_{avg} is the average speed of vehicle driving along the given route, which is determined by the historical data. a_d and a_b are the desired acceleration and deceleration, respectively, which meet the driving comfort requirements. Then, $\mathbb{t}_p^k \in \mathbb{N}^+ = \left[t_{p\_min}^{k}: 1: t_{p\_max}^{k}\right]$ if the sampling time is 1 s.

In addition, the incoming time at each intersection segment (i.e., $[S^{k-1}, S^k]$) should be mapped into the global time domain. When $k = 1$ that corresponds to the first intersection segment, the incoming time is the start time of the entire mission. For $k > 1$, the incoming time of the kth intersection segment equals the crossing time of the vehicle at the previous intersection $k - 1$. Therefore, the incoming time at each intersection segment is expressed by Eq. (20).

$$\mathbb{t}_a^k = \begin{cases} 0 & k = 1 \\ \left[\sum_{j=1}^{k-1} t_{p\_min}^{j} : 1 : \sum_{j=1}^{k-1} t_{p\_max}^{j}\right] & k > 1 \end{cases} \tag{20}$$

where $\mathbb{t}_a^k \in \mathbb{N}$ is the set of incoming times in the kth intersection segment. Eqs. (18)-(20) reveal the relationship between the incoming and passing times at an intersection and it can be observed that the sets of incoming and passing times have the same size. Then, by using the traffic signal model summarized in Eq. (4), the set of feasible green windows $\mathbb{C}^k$ is calculated using Eq. (21).

$$\mathbb{C}^k = \left[\text{ceil}\left(\frac{\min(\mathbb{t}_a^k) + \min(\mathbb{t}_p^k) - T_0^k}{T_l^k}\right) + 1, \text{ceil}\left(\frac{\max(\mathbb{t}_a^k) + \max(\mathbb{t}_p^k) - T_0^k}{T_l^k}\right)\right] \tag{21}$$

Fig. 9 shows the typical sets of green windows for a vehicle driving through three signalized intersections, where the dotted gray lines represent potential driving profiles. The set of the feasible green window for intersections are $\mathbb{C}^1 = [2, 3]$, $\mathbb{C}^2 = [3, 4, 5, 6]$ and $\mathbb{C}^3 = [2, 3, 4]$. Instead of directly minimizing the travel time, this section searches for the shortest path for green windows, that is, the green window planning problem is transformed into a directed graph representation. Then, the shortest path problem is formulated to derive the shortest path from S_1 to S_{N_t} (a series of C^k subject to the feasible set $\mathbb{C}_k$ for each signal) to minimize the travel time:

$$\underset{\{C^k \in \mathbb{C}_k\}_{k=1}^{N_t}}{\text{Minimize}} \quad J = \sum_{i=1}^{N_t} C^i \tag{22}$$

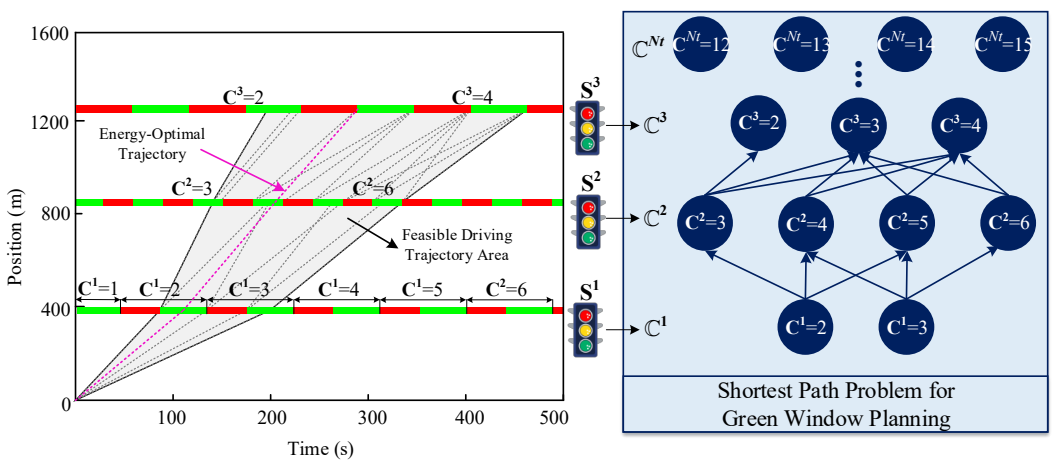

Fig. 9. Typical example of possible green windows for a vehicle driving through three signalized intersections

4.2 Heuristic A algorithm*

This study uses the A* algorithm [39] to solve the shortest path problem formulated in Eq. (22). We defined each intersection as a node, as shown in Fig. 9, and the path cost of the current node is the number of traffic signal cycles C^i. Then, the evaluation function $\Psi(j)$ of the A* algorithm is calculated using Eq. (23).

$$\Psi(j) = g_c(j) + h_c(j) \tag{23}$$

where $g_c(j)$ is the exact cost at the jth node, and $h_c(j)$ is the heuristically estimated cost from jth traffic signal to the last one. More specifically, $g_c(j)$ is the sum of the optimal signal cycles, $C_{p\_opt}^k$, from the first intersection to the current intersection along the selected optimal path, as shown in Eq. (24)

$$g_c(j) = \sum_{1}^{j} C_{p\_opt}^j \tag{24}$$

and $h_c(j)$ is the minimum sum of signal cycles from the jth to the last node,

$$h_c(j) = \min \sum_{j}^{N_t} C_p^j \tag{25}$$

where C_p^j is an associated feasible traffic signal cycle. In the A* algorithm, the heuristic function $h_c(j)$ directly affects the optimal path searching performance. Suppose that the exact cost from the jth node to the final node is $H(j)$. $h_c(j) < H(j)$ suggests that many search paths cause low operation efficiency, but the optimal path can be searched; if $h_c(j) > H(j)$, there are fewer search paths and the calculation efficiency is high, but it is usually difficult to find the optimal path. Otherwise, $h_c(j) = H(j)$ represents an ideal situation in which the search is performed along the shortest path with the highest efficiency. Thus, substituting Eq. (21) into Eq. (25), the heuristic cost function for green window prediction is accessed.

Ultimately, the efficient green window sequence $\mathbb{C}_{p\_opt}$ and time interval sequence $\mathbb{T}_{p\_opt}$ are obtained, that is, $\mathbb{C}_{p\_opt} = [C_{p\_opt}^1, \cdots, C_{p\_opt}^{N_t}]$ and $\mathbb{T}_{p\_opt} = \{[T_{p\_min}^1, T_{p\_max}^1], \cdots, [T_{p\_min}^{N_t}, T_{p\_max}^{N_t}]\}$, where, $T_{p\_min}^j$ and $T_{p\_max}^j$ are the starting and ending times of efficient green window, respectively, which are calculated using Eqs. (26) and (27), respectively.

$$T_{p\_min}^j = \max\left(t_{p\_min}^j, t_{g,C_{p\_opt}^j}^j\right) \tag{26}$$

$$T_{p\_max}^j = \min\left(t_{p\_max}^j, t_{g,C_{p\_opt}^j}^j + T_g^j\right) \tag{27}$$

5. Predictive Speed Optimization

Taking the derived efficient green windows as the input for speed optimization, this section optimizes the speed trajectory in the spatial domain. The RHVO strategy focuses on minimizing energy consumption and prolonging battery life while meeting the driving comfort requirements.

5.1 Distance-based Receding Scheme and Optimal Control Problem

The proposed RHVO divides the entire route into multiple phases in the spatial domain. Each intersection segment is defined as one phase, and the adjacent phases are connected by boundary conditions (vehicle speed, and travel time). The receding optimization phase of the entire route equals the number of intersections, that is, $k = 1,2,\ldots,N_t$. In each receding optimization phase, the vehicle initial states are the terminal states of the previous phase, that is, $v^k(0) = v^{k-1}(S^{k-1})$ and $t^k(0) = t^{k-1}(S^{k-1})$. Note that the initial states of the vehicle in the first phase are defined as the

vehicle states when the trip starts. In addition, the terminal time is subjected to the efficient green window intervals derived from Section 4, that is, $T_p^k \in \left(T_{p\_min}^k, T_{p\_max}^k\right)$.

Because the route distance is fixed for any route $\mathcal{R}$, the time-domain OCP (Eqs. (16) and (17)) is transformed into the spatial domain as shown in Eq. (28).

$$\underset{u\in U}{\text{Minimize}} \quad J\big(u(n),x(n)\big) = \alpha_1 \sum_{n=1}^{n=l} \left(P_{m_{loss}}(n) + P_{b_{loss}}(n)\right) t_D(n) + \alpha_2 \sum_{n=1}^{n=l} Q_{loss}(n)\, t_D(n) + \alpha_3 \sum_{n=1}^{n=l} |\Delta a(n)| \tag{28}$$
$$+\alpha_4 (v(l) - \min(v_{max}^k, v_{max}^{k+1}))^2 + \alpha_5 \left(t(l) - T_{p\_min}^k\right)^2$$

s.t.

$$u_{min}(n) \le u(n) \le u_{max}(n)$$
$$v_{min}^k \le v(n) \le v_{max}^k$$
$$T_{p\_min}^k \le t(l) \le T_{p\_max}^k$$
$$v(n) = \sqrt{v^2(n-1) + 2a(n)\Delta d}$$

where Δd is the sampling distance. l is the total number of distance steps, that is, $l = D^k/\Delta d + 1$. α_* is the weighting factor for the different objectives. $x(n)$ is the state vector, that is, $x(n) = [v(n), t(n)]^T$, and $u(n)$ is the control input, that is, $u(n) = F_v(n)$. $t_D(n)$ is the time required to travel from $(n-1)$th distance step to the next and is approximated using Eq. (29).

$$t_D(n) = \frac{\Delta d}{0.5(v(n-1) + v(n))} \tag{29}$$

For ease of computation, the terminal distance and velocity conditions in Eqs. (17) are converted into the soft constraints in Eq. (28) with α_4 and α_5 weighting factors for the latter terms, which can drive the states to the desired terminals. In addition, the travel time of the host vehicle in the kth phase is limited by $T_{p\_min}^k$ and $T_{p\_max}^k$.

5.2 Iterative Dynamic Programming

This subsection uses IDP to solve the formulated OCP. Principally, IDP involves refining the search space iteratively to improve the calculation efficiency of the regular DP algorithm [40]. For a regular DP, the transitional cost-to-go function from k to step $k+1$ $L\big(u(k),x(k)\big)$ and the penalty function for the terminal states $G_N(x(n))$ are defined in Eqs. (30) and (31), respectively.

$$L\big(u(k),x(k)\big) = \alpha_1 \left(P_{m\_loss}(k) + P_{b\_loss}(k)\right) \Delta t_D + \alpha_2 Q_{loss}(k)\Delta t_D + \alpha_3 |\Delta a(k)| \tag{30}$$

$$G_N\big(x(n)\big) = \alpha_4 (v(n) - \min(v_{max}^k, v_{max}^{k+1}))^2 + \alpha_5 \left(t(n) - T_{p\_min}^k\right)^2 \tag{31}$$

The formulated OCP is solved recursively by following the Bellman Principle [41].

$n-1$ step:

$$J_{n-1}\big(x(n-1)\big) = \min_{u\in U}[L\big(u(n-1),x(n-1)\big) + G_N(x(n))] \tag{32}$$

k step:

$$J_k\big(x(k)\big) = \min_{u\in U}[L\big(u(k),x(k)\big) + J_{k+1}^*(x(k+1))] \tag{33}$$

where $J_k\big(x(k)\big)$ is the minimum cost-to-go value at the moment k.

To reduce the computational burden of DP, the grid size of vehicle states and control input can be increased. However, a coarse grid may affect the calculation accuracy. This study proposes a new dynamic programming algorithm with boundary tuning and grid size scaling strategies, IDP, to realize a trade-off between calculation speed and accuracy. The mesh generation principle of the IDP is shown in Fig. 10, in which coarse grids are first employed, and the density of the grid points and the feasibility region of states and control input change gradually to recursively derive the optimal solution.

In the first iteration, a coarse grid is defined (Δx_1 and Δu_1) to find the optimal control rule $u_{opt,1}$ and state trajectory

$x_{opt,1}$. Then, the boundaries of the control inputs and states in the $(i+1)$th iteration $(x_{min,i+1}, x_{max,i+1})$ and $(u_{min,i+1}, u_{max,i+1})$ are determined using the results of the previous iteration, respectively,

$$x_{min,i+1} = \max\left(x_{optL,i} - \tau\Delta x_i, x_{min}\right),\ x_{max,i+1} = \min\left(x_{optU,i} + \tau\Delta x_i, x_{max}\right) \tag{34}$$

$$u_{min,i+1} = \max\left(u_{optL,i} - \sigma\Delta u_i, u_{min}\right),\ u_{max,i+1} = \min\left(u_{optU,i} + \sigma\Delta u_i, u_{max}\right), \tag{35}$$

where $x_{optU,i}$, $x_{optL,i}$, $u_{optU,i}$ and $u_{optL,i}$ are the maximum and minimum values of the state and control input at the *i*th iteration, respectively. $\tau \le 1$ and $\sigma \le 1$ are the boundary tuning factors for the constraints of the state and control variables, respectively. Δx_i and Δu_i are the grid sizes for the *i*th iteration, respectively, which are defined by scaling factors $\gamma < 1$ and $\lambda < 1$, that is, $\Delta x_{i+1} = \gamma\Delta x_i$ and $\Delta u_{i+1} = \lambda\Delta u_i$.

Consider the maximum number of allowed iterations I_{max}. The IDP algorithm terminates when the following conditions are satisfied,

$$E_{opt,i} \le \vartheta E_{opt,i-1} \text{ or } i > I_{max} \tag{36}$$

where $E_{opt,i}$ is the optimized energy consumption, and ϑ is the leverage factor of the IDP's accuracy and convergence speed. In other words, the IDP continuously rescales and solves the resulting OCP unless the solution converges or the maximum number of iterations is reached. The convergence of the IDP to a global or near-to-global optimum is shown in [40]. Notably, the parameters τ, σ, γ, λ, and ϑ can affect the calculation speed and optimization accuracy. From the IDP calculation, the vehicle optimal state profile $\mathbb{x}_s$ and control input profile $\mathbb{u}_s$ in each phase can be obtained. The implementation algorithm for IDP is presented in Algorithm 1.

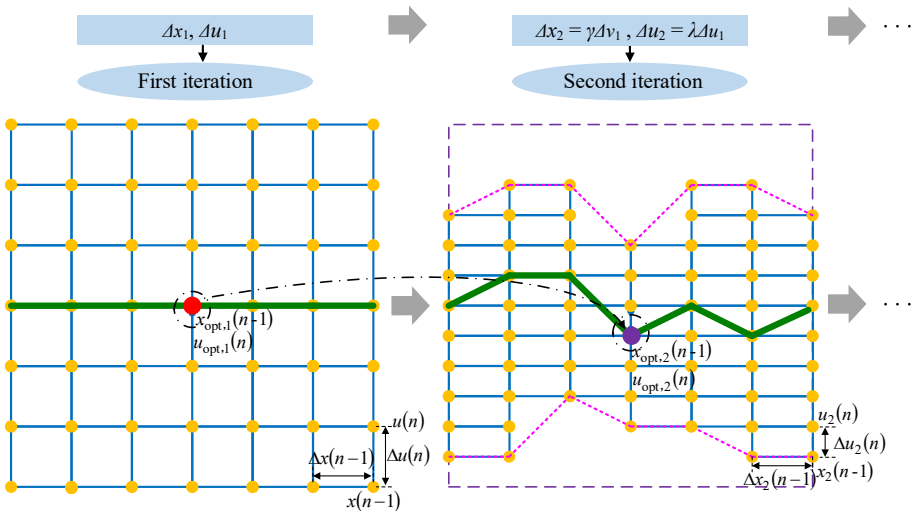

Fig. 10. Mesh generation principle of proposed IDP. Note that the green line is the optimal solution.

Algorithm 1 Implementation algorithm for the IDP

Input: $v(0)$, $t(0)$, $d(0)$, $u(0)$, T_{p_min}, T_{p_max}, ϑ, I_{max}, x_{max}, x_{min}, u_{max}, u_{min}, τ, σ, γ, λ, Δx, Δu, l, ϑ
Output: $\mathbb{x}_s$, $\mathbb{u}_s$
1. Initial by setting $i = 1$, $x_{min,1} = x_{min}$, $x_{max,1} = x_{max}$, $u_{min,1} = u_{min}$, $u_{max,1} = u_{min}$, $\Delta x_1 = \Delta x$, $\Delta u_1 = \Delta u$
2. **while** $E_{opt,i} \le \vartheta E_{opt,i-1}$ or $i > I_{max}$
3. Mesh generation $x = [x_{min,i}: \Delta x_i: x_{max,i}]$, $u = [u_{min,i}: \Delta u_i: u_{max,i}]$
4. **for** $n = l: -1: 1$
5. Reverse optimization based on the Bellman Principle in Eqs. (30)-(33)
6. Calculate the optimal control policy
7. **end for**
8. **for** $n = 1: 1: l$
9. Forward calculation with vehicle initial states $v(0)$, $t(0)$, $d(0)$, $u(0)$
10. Obtain the vehicle optimal states set $\mathbb{x}_i$, the control input set $\mathbb{u}_i$, and $E_{opt,i}$
11. **end for**
12. Set $x_{optU,i} \leftarrow \max(x_i)$, $x_{optL,i} \leftarrow \min(x_i)$, $u_{optU,i} \leftarrow \max(u_i)$, $u_{optL,i} \leftarrow \min(u_i)$
13. Redefine bounds of states $x_{max,i+1} \leftarrow \min\left(x_{optU,i} + \tau\Delta x_i, x_{max}\right)$, $x_{min,i+1} \leftarrow \max\left(x_{optL,i} - \tau\Delta x_i, x_{min}\right)$
14. Redefine bounds of control inputs $u_{max,i+1} \leftarrow \min\left(u_{optU,i} + \sigma\Delta u_i, u_{max}\right)$, $u_{min,i+1} \leftarrow \max\left(u_{optL,i} - \sigma\Delta u_i, u_{min}\right)$
15. Scale state and control input grids $\Delta u_{i+1} \leftarrow \lambda\Delta u_i$, $\Delta x_{i+1} \leftarrow \gamma\Delta x_i$
16. $i \leftarrow i + 1$
17. **end while**
18. Set $\mathbb{x}_s \leftarrow \mathbb{x}_i$, $\mathbb{u}_s \leftarrow \mathbb{x}_i$

The vehicle optimal states set $\mathbb{x}_{opt}$ and control input set $\mathbb{u}_{opt}$ in the entire route after completing the optimization at each stage using the IDP are denoted by Eqs. (37) and (38), respectively:

$$\mathbb{x}_{opt} = \left[\mathbb{x}_s^1, \cdots, \mathbb{x}_s^{N_t}\right] \tag{37}$$

$$\mathbb{u}_{opt} = \left[\mathbb{u}_s^1, \cdots, \mathbb{u}_s^{N_t}\right] \tag{38}$$

For clarity, the RHVO solution at multiple intersections is summarized in Algorithm 2.

Algorithm 2 Implementation algorithm for the RHVO

Input: N_t, $\mathbb{S}_t$, $\mathbb{V}_{max}$, $\mathbb{V}_{min}$, u_{max}, u_{min}, $\mathbb{T}_{p\_opt}$
Output: $\mathbb{x}_{opt}$, $\mathbb{u}_{opt}$
1. Initial by setting $k = 1$
2. **while** $k \leq N_t$
3. **if** $k = 1$
4. Initial by setting $l = D^k/\Delta d + 1$, $v^1(0) = v_s$, $t^1(0) = 0$, $d^1(0) = 0$, $u^1(0) = 0$
5. **else**
6. Initial by setting $l = D^k/\Delta d + 1$, $v^k(0) = v^{k-1}(l)$, $t^k(0) = t^{k-1}(l)$, $d^k(0) = d^{k-1}(l)$, $u^k(0) = u^{k-1}(l)$
7. **end if**
8. $(\mathbb{x}_s^k, \mathbb{u}_s^k)$ = IDP $(v^k(0), t^k(0), d^k(0), u^k(0), T_{p\_min}^k, T_{p\_max}^k, I_{max}, x_{min}^k, x_{max}^k, u_{min}^k, u_{max}^k, \tau, \sigma, \gamma, \lambda, \Delta x, \Delta u, l, \vartheta)$
9. $k \leftarrow k+1$
10. **end while**
11. Set $\mathbb{x}_{opt} \leftarrow \left[\mathbb{x}_s^1, \cdots, \mathbb{x}_s^{N_t}\right]$, $\mathbb{u}_{opt} \leftarrow \left[\mathbb{u}_s^1, \cdots, \mathbb{u}_s^{N_t}\right]$

6. Simulation and Results

To evaluate the benefits of the proposed M-EAD strategy, several simulations were conducted on a PC with an Intel Core i7-8700 @ 3.20GHz CPU and 16GB RAM. The M-EAD strategy is first compared to the benchmark strategies in a given route with complete SPaT information and then evaluated using Monte Carlo simulation, in which the traffic signal initial states were random in each stochastic simulation.

6.1 Given Route and Simulation Setup

The test route is located at Jiangjun Avenue, Nanjing, China, and an overview of the path is shown in Fig. 11. The total length of the route is 6794 m. The SPaT of all traffic signals along the route is fixed, as summarized in Table 1. The main EVs parameters are listed in Table 2. The sampling distance in RHVO was 5 m. The weighting factors of the OCP in Eqs. (28) are set to $\alpha_1 = 1$, $\alpha_2 = 2 \times 10^9$, $\alpha_3 = 0.1$, $\alpha_4 = 0$ or 10^{10}, and $\alpha_5 = 200$, which find a good compromise between vehicle energy efficiency, travel time, battery life, and driving comfort, as verified by a systematic simulation analysis for various weight factors.

Table 1

Information on traffic signal and road speed limit.

ID	Location S (m)	Green signal interval T_g (s)	Signal cycle time T_l (s)	Initial states		Maximum speed v_{max} (km/h)	Minimum speed v_{min} (km/h)
				Signal indication P	Transition time T_s (s)		
1	460	28	97	Red	26	60	30
2	1060	50	77	Green	46	60	
3	1625	48	97	Red	9	60	
4	2315	30	104	Green	8	60	
5	3015	40	86	Green	6	50	
6	3325	35	79	Green	5	50	
7	3945	34	105	Red	62	60	
8	4865	35	110	Red	43	60	
9	5740	35	97	Red	34	70	
10	6790	45	89	Green	7	70	

Furthermore, we conducted a systematic analysis to obtain the parameter group of the IDP with respect to the trade-off between computational efficiency and optimization accuracy. The sampling distance (5 m) and time grid size (0.1 s) in the IDP are fixed, and the vehicle speed grid size (initial value is 10 km/h) and the control force grid size (initial value is 50 N) are iteratively scaled. The scaling factors are $\tau = 0.4$, $\sigma = 0.3$, $\gamma = 0.02$, and $\lambda = 0.3$. The allowance factor ϑ is set as 0.95, that is, the iteration will stop when the step improvement of IDP is less than 5%.

6.2 Benchmark Strategies

The proposed M-EAD strategy is compared with two existing strategies: CS and I-EAD [18] for benchmarking purposes. In the CS strategy, the host vehicle approaches and departs from the intersection at a constant cruising speed. The constant cruising speed is the average speed of the proposed M-EAD strategy. When the traffic signal is red, the vehicle decelerates to a stop and accelerates to pass through the intersection when the traffic signal turns green. The vehicle acceleration and deceleration are defined as 2 m/s^2 and –2 m/s^2, respectively, and the standstill spacing between the stop line is 0 m when blocked by a red sign. The I-EAD strategy uses the isolated intersection SPaT information to calculate the energy-optimal passing through speed as introduced in Section 3.1. In addition, when the average speed of a vehicle passing through the intersection stop line at the start of the green signal is lower than the minimum speed limit, we define this as a stopping inevitable condition. Then, the I-EAD optimizes the energy-optimal stopping speed to arrive at the intersection stop line.

Table 2

Vehicle parameters.

Component	Parameter	Value
Motor	Maximum torque	120 Nm
	Maximum speed	8000 rpm
Li-ion Battery	Rated capacity Q_b	52.8 Ah
	Open circuit voltage V_{oc}	360 V
	Ideal gas constant R	8.31
	Exponential factor z	1.82
Vehicle	Mass m	1005 kg
	Front area A	2.02 m^2
	Air drag coefficient C_D	0.3
	Air density ρ	1.206 kg/m^3
	Rotational inertia coefficient δ	1.022
	Rolling resistance coefficient f	0.015
	Tire radius r_w 165/65 R15	0.280 m
	Accessory power P_a	300 W
	Acceleration of gravity g	9.8 m/s^2
	Transmission ratio i_t	10.609
	Desired acceleration a_d	2 m/s^2
	Desired deceleration a_b	− 2 m/s^2
	Initial velocity v_s	50 km/h

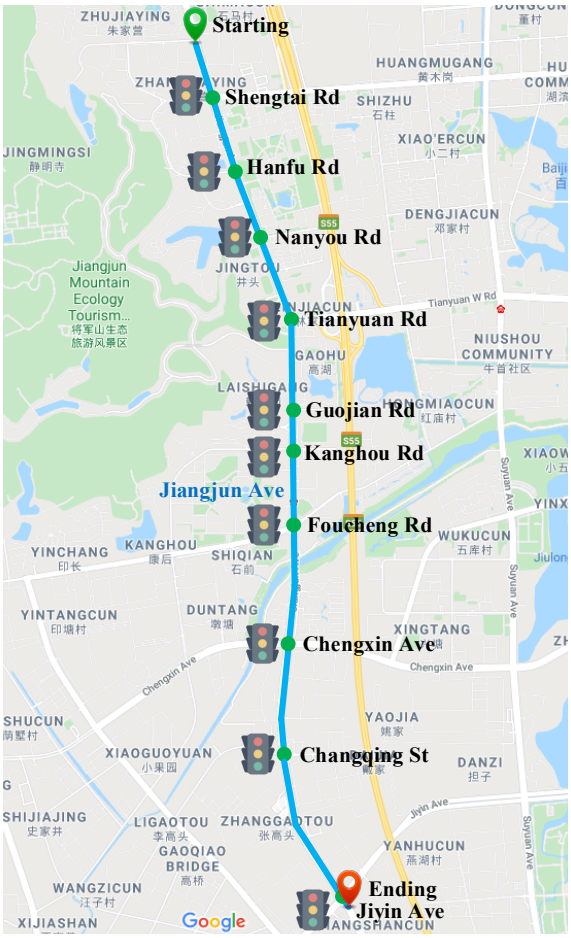

Fig. 11. Urban network map of Jiangjun Avenue, Nanjing, China.

6.3 Simulation Results

Table 3 lists the optimized efficient green windows. As observed, the time interval of the efficient green window was

mostly less than the corresponding full green window interval. If the host vehicle can cross the intersection at the start time of an efficient green window, the travel delay will be further reduced. However, it may be difficult to achieve a trade-off between mobility and energy efficiency. Therefore, two sub-strategies are proposed based on the control purposes, that is, M-EAD A and M-EAD B. In M-EAD A, the start time of an efficient green window is defined as a terminal constraint, to ensure that host vehicles pass through intersections with optimal time-saving speed. In M-EAD B, the intersection passing time is relaxed and only restricted within the range of an efficient green window interval, thus achieving the energy-optimal goal. For a fair comparison, two versions of the CS strategy are defined: CS (M-EAD A) and CS (M-EAD B), which correspond to the average speed in M-EAD A and M-EAD B, respectively.

Table 3

Results of green window planning.

Intersection ID	1	2	3	4	5	6	7	8	9	10
Efficient traffic signal cycle	1	2	2	3	4	5	3	4	5	7
Full green window interval (s)	[27, 54]	[74, 123]	[107, 154]	[187, 216]	[225, 264]	[231, 265]	[273, 306]	[374, 408]	[423, 457]	[497, 541]
Efficient green window interval (s)	[29, 54]	[74, 113]	[109, 148]	[187, 191]	[238, 242]	[261, 265]	[299, 306]	[374, 408]	[423, 457]	[497, 541]

6.3.1. Computational burden reduction of IDP

The benefit of IDP in terms of computational efficiency compared to DP is revealed in this subsection. The range of the vehicle speed and control force for optimization are shown in Figs. 12 and 13, respectively. As observed, compared to DP, IDP can reduce boundary ranges, thereby reducing computational complexity. From the computation time and the resulting cost listed in Table 4, IDP can improve the calculation speed by 89 % compared to DP, whereas the optimality is sacrificed by only 3.88 %.

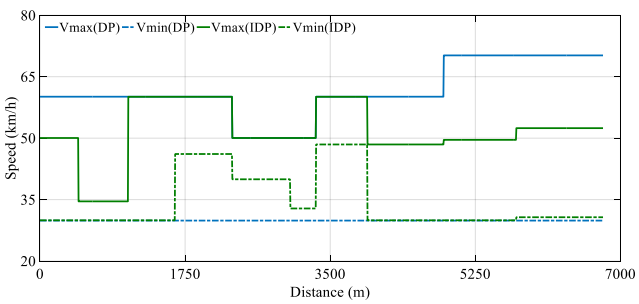

Fig. 12. Boundary of vehicle speed.

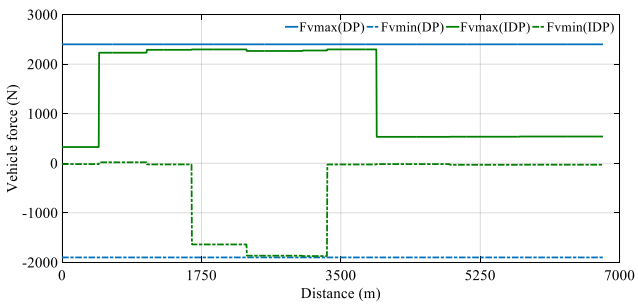

Fig. 13. Boundary of vehicle control force.

Table 4

Comparison between the DP and IDP.

Parameter	Calculation time		Cost	
	Value	Reduction	Value	Increase
DP	2152.3 s	—	53112.89	—
IDP	236.8 s	89 %	55171.84	3.88 %

6.3.2. Effectiveness of proposed M-EAD strategy

Now, we compare the M-EAD against two benchmark strategies, CS and I-EAD, to further verify the effectiveness of the M-EAD. Figs. 14-16 show the profiles of the travel distance, vehicle speed, vehicle acceleration/deceleration of the CS, I-EAD, M-EAD A, and M-EAD B strategies. Tables 5 and 6 list the values and comparison results of energy consumption, travel time, and battery capacity loss obtained from each method, respectively. Notably, different strategies may result in different final driving speeds at the destination. To make a fair comparison, the total energy consumption of each strategy combines both the consumed energy and the differences between the initial and terminal kinetic energy of the vehicle.

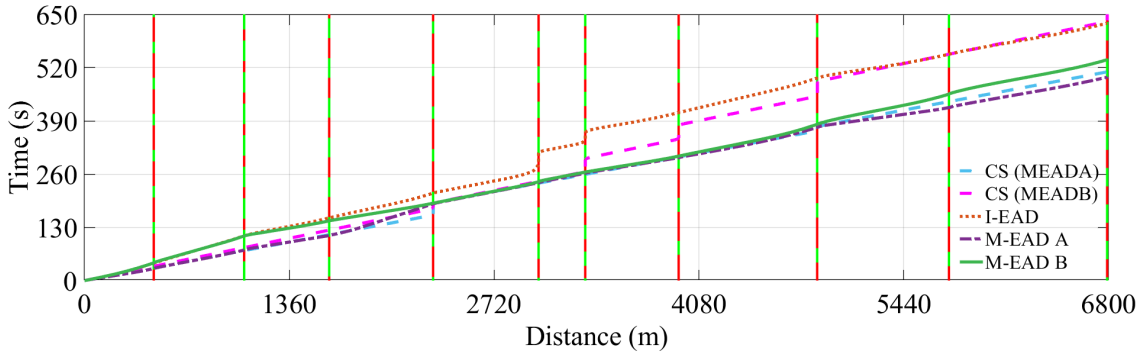

Fig. 14. Travel distance profile in simulation.

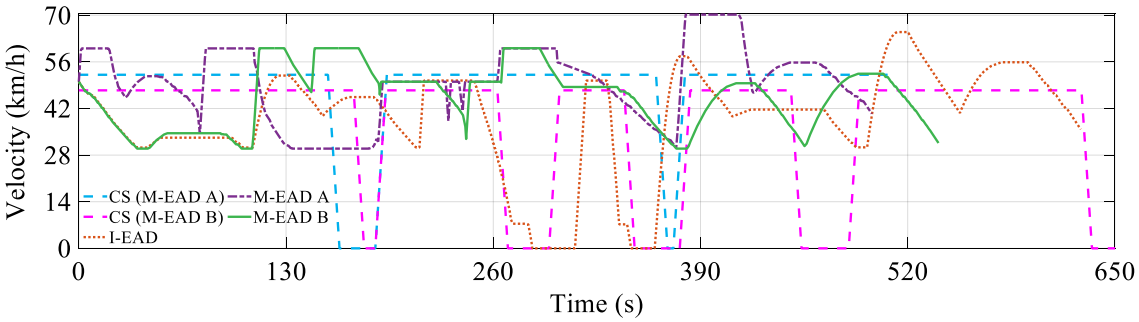

Fig. 15. Vehicle speed profile in simulation.

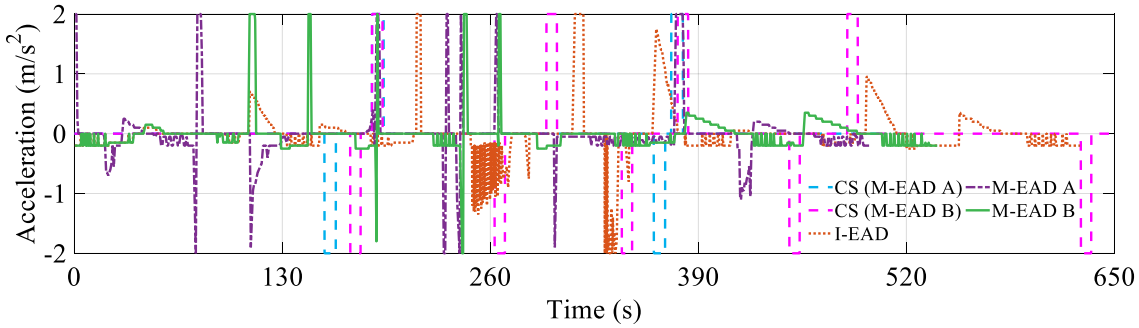

Fig. 16. Vehicle acceleration/deceleration profile in simulation.

TABLE 5

Simulation results for CS, I-EAD, and M-EAD strategies.

Strategy	CS (M-EAD A)	CS (M-EAD B)	I-EAD	M-EAD A	M-EAD B
Energy Consumption	2589.41 kJ	2287.13 kJ	2068.54 kJ	2565.84 kJ	1911.93 kJ
Travel time	510.2 s	673.9 s	628.6 s	497.5 s	539.3 s
Battery capacity loss	0.0016 %	0.0015 %	0.0014 %	0.0016 %	0.0013 %

TABLE 6

Energy efficiency, travel time, and battery life comparison for CS, I-EAD, and M-EAD strategies.

Strategy		CS (M-EAD A)	CS (M-EAD B)	I-EAD
Energy efficiency improvement	M-EAD A	0.91 %	—	-24.04 %
	M-EAD B	—	16.40 %	7.57 %
Travel time reduction	M-EAD A	2.48 %	—	20.86 %
	M-EAD B	—	19.97 %	14.21 %
Battery life extending	M-EAD A	0 %	—	-14.29 %
	M-EAD B	—	13.33 %	7.14 %

As shown in Figs. 14 and 15, the host vehicle in CS (M-EAD A), CS (M-EAD B), and I-EAD were blocked by the red signal at the 3rd and 8th intersections; 4th, 6th, 7th, 8th, and 10th intersections; and 5th and 6th intersections, respectively. In contrast, both M-EAD A and M-EAD B drove through all intersections without stopping. In Tables 5and 6, both M-EAD A and M-EAD-B achieved travel time reductions compared to the CS and I-EAD strategies. However, the energy consumption for M-EAD A is higher than that of CS, whereas M-EAD B achieves both energy consumption and travel time reduction, compared with CS. Compared to M-EAD A, M-EAD B reduced the energy consumption by 25.49 % with only an 8.4 % travel time extension. In addition, the battery capacity loss for the three strategies corresponds to their energy efficiencies.

A plausible explanation for these results is that the vehicle at CS needs to stop at the intersection (see Fig. 14). Although the I-EAD can optimize the energy-optimal speed by utilizing the isolated intersection SPaT information, it is incapable of passing every intersection without stops because it neglects the spatial-temporal correlation among intersections (see Fig. 14); thus, the travel time was also extended. The large changes in velocity are inevitable in the stop-and-go operation (see Fig. 15); therefore, the energy consumption of CS and I-EAD is higher than that of M-EAD B. The M-EAD A and B strategies both optimize the efficient green window at the beginning of the trip for travel delay reduction. Since the shorter travel time corresponds to a higher average driving speed that tends to increase energy usage, the energy consumption of M-EAD A is higher than M-EAD B, which represents a compromise solution method between energy efficiency and travel time. In addition, the vehicle velocity and acceleration/deceleration profiles of M-EAD B are smoother than those of CS, I-EAD, and M-EAD A strategies with improved overall energy efficiency.

Owing to the coordination superiority of vehicle energy saving and traffic efficiency of M-EAD B, M-EAD B is assumed to be representative of the proposed M-EAD strategy, and abbreviated "M-EAD." Although the effectiveness of the M-EAD is promising, it is not clear if significant improvement in average vehicle energy efficiency and travel time reduction can be achieved with the M-EAD if the initial states in all traffic signals are varied. In the following subsection, we discuss the average effects of the proposed method.

6.4 Performance Discussion of M-EAD Strategy with Stochastic Traffic Signal Initial States

In reality, the fixed SPaT of traffic signals is easy to access, but the initial states of multiple traffic signals are difficult to obtain synchronously. Therefore, to elucidate the average effects of the proposed method, we conducted a series of stochastic simulations. We evaluate a statistically significant number of cases with randomly generated initial states, which is a variant of a Monte Carlo simulation. The investigation involved 600 individual simulation trials for the given test route. The initial signal indication and transition time were randomized, and the full cycle length, red and green indication intervals were kept constant. The histograms of the improvement of energy consumption, travel time reduction, and battery capacity loss reduction of 600 stochastic tests are shown in Figs. 17-19. The average improvement results of the energy consumption, travel time, and battery capacity loss are summarized in Table 7.

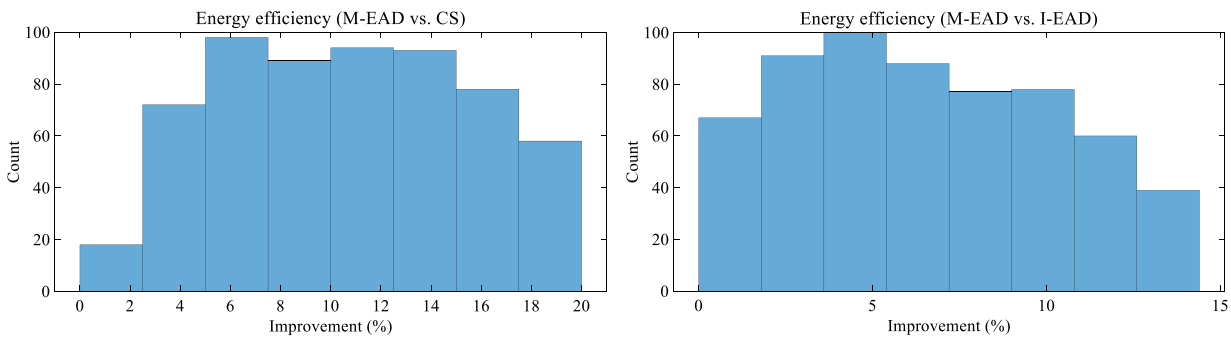

(a) M-EAD vs. CS (b) M-EAD vs. I-EAD

Fig. 17. Energy economy improvement during 600 stochastic simulations.

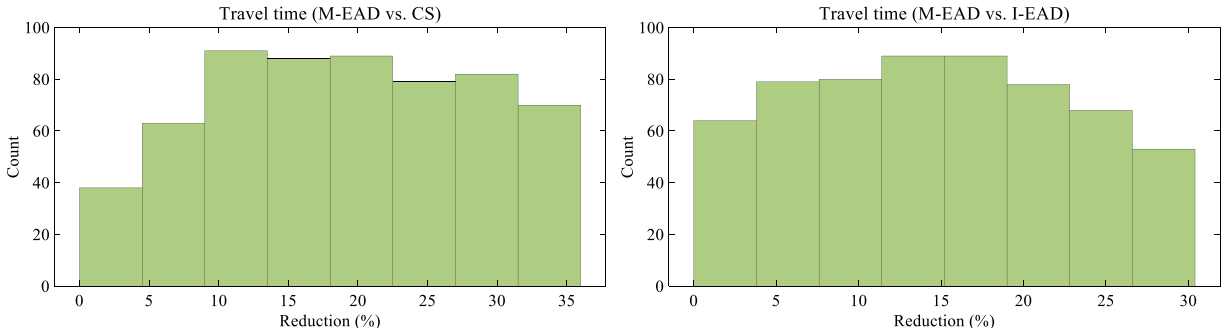

(a) M-EAD vs. CS (b) M-EAD vs. I-EAD

Fig. 18. Travel time reduction during 600 stochastic simulations.

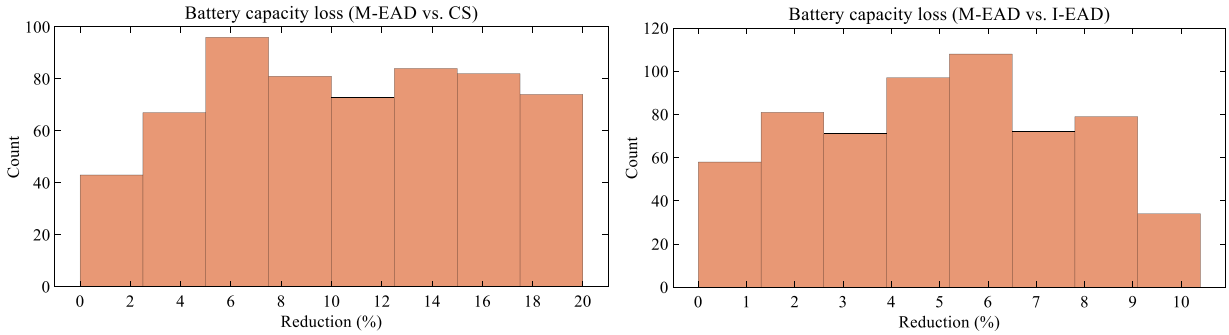

(a) M-EAD vs. CS (b) M-EAD vs. I-EAD

Fig. 19. Battery capacity loss reduction during 600 stochastic simulations.

Table 7

Average energy efficiency improvement, travel time reduction, and battery capacity loss reduction during 600 stochastic simulations.

	Average energy efficiency improvement	Average travel time reduction	Average battery capacity loss reduction
M-EAD vs. CS	10.65 %	19.04 %	10.51 %
M-EAD vs. I-EAD	6.55 %	14.79 %	5.01 %

As shown in Figs. 17-19, the energy efficiency improvement, travel time reduction, and battery capacity loss reduction for the M-EAD are dispersed. Compared with CS, the minimum and maximum improvements in terms of energy efficiency, travel time, and battery capacity loss of M-EAD are 1.84 % and 19.98 %, 1.18 % and 35.95 %, and 1.03 % and 20.00 %, respectively. When compared with I-EAD, M-EAD can reduce the vehicle energy consumption, travel time, and battery lifetime degradation by up to 13.95 %, 29.93 %, and 10.00 %, respectively, when compared with I-EAD. The superiority of the proposed M-EAD may be attributable to the traffic signal conditions. Specifically, whether to stop and the number of stops in a route is related to the initial signal indication and transition time of the traffic lights. For example, when the vehicle excludes the stop operations of CS and I-EAD strategies, the energy consumption, travel time, and battery capacity loss of the three strategies are similar; therefore, the advantage is not prominent in the M-EAD strategy. However, if the vehicle includes the stop operations of the CS and I-EAD strategies, as displayed in Section 6.3, the advantages of the energy economy, time savings, and battery life extension in M-EAD are evident.

In addition, the results in Table 7 indicate that, for the test route described and with stochastic initial states of traffic signals, an average of 10.65 %, 19.04 %, and 10.51 % increase in the energy economy, travel time saving, and battery life can be expected compared with the CS strategy, and 6.55 %, 14.79 %, and 5.01 %, respectively, compared with the I-EAD strategy. These results indicate that the proposed M-EAD has marked advantages in terms of energy economy and traffic efficiency, and its robustness in stochastic traffic scenarios is good.

7. Experiment and Results

7.1 Facilities

A field test was conducted based on a developed CAV platform, Chery Little-Ant as shown in Fig. 20. The CAV is equipped with a global navigation satellite system/inertial navigation system, millimeter-wave radar, LiDAR, several cameras, V2I device, and an on-board computing platform with an Intel Core i7-7700 @ 3.6GHz CPU. The global navigation satellite system/inertial navigation system provides precise positioning information, and the initial SPaT information of all downstream intersections can be accessed by an on-board V2I device via 4G communication. Because all signal controllers along the test route are operated in a fixed-time strategy, the future signal states can be predicted. Using the acquired information, the proposed M-EAD calculates the optimized speed profile, which is sent to the lower-level vehicle controller. Then, the test vehicle controls the traction motor and braking system to maintain the optimized speed using the Proportion-Integration-Differentiation controller. The communication and control framework of the test vehicle is shown in Fig. 21, it is based on the Robot Operating System. In addition, the experimental results, including vehicle speed, position, and SOC were recorded at 20 Hz.

The test route is the same as that used in the simulation, as shown in Fig.11. The test vehicle received all traffic signal information 1000 m ahead of the starting position, including positions of an intersection stop line, traffic signal phases and timing, and speed limits. The driving lane, starting and ending positions for the host vehicle were defined before the experiment. The process of the experiment is as follows: 1) The M-EAD strategy is triggered for optimal speed derivation while the traffic signal information is received with V2I communication. Before entering the test zone, the vehicle is controlled by the driver, who drives the vehicle at a pre-defined speed. The human machine interface prompts the driver to arrive at the start position of the test road at the appointed time and defined speed. 2) Once the vehicle reached the marked starting position of the test road, the automated driving mode is activated manually, and the test vehicle is controlled to follow the pre-defined driving trajectory and optimized speed. The experiment results, including host vehicle speed, position, and battery SOC are recorded. 3) When the test vehicle passes the ending position of the test road, the experiment and data recording mode are terminated. After that, the driver will take over the control of the vehicle. Noted that in step 2 of the experiment, the requirement to reach the starting position at the specified time and speed may be strong. To impose this, we first found the time consumption of calculating the optimal vehicle speed through the preliminary test, which required about 250 s. In this context, we stipulate the arrival time of the test vehicle at the starting point is 280 s. Based on the traffic light model, initial states, and SPaT information, the optimal speed trajectory from 280 s is calculated. The cruise speed is 10 km/h before the optimal speed is derived. After that, the driver adjusts the speed based on experience and reaches the starting point at about 280 s.

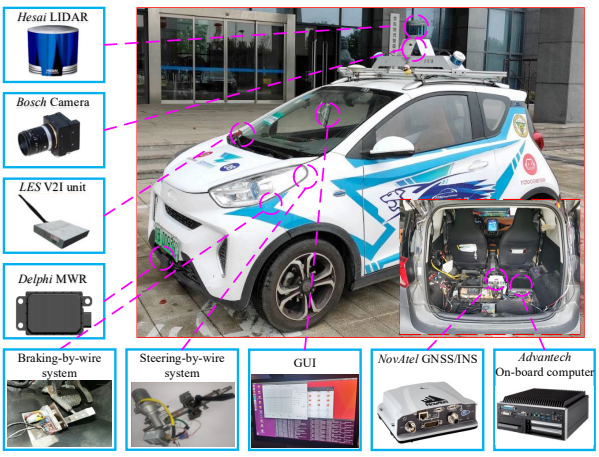

Fig. 20. The CAV experiment platform.

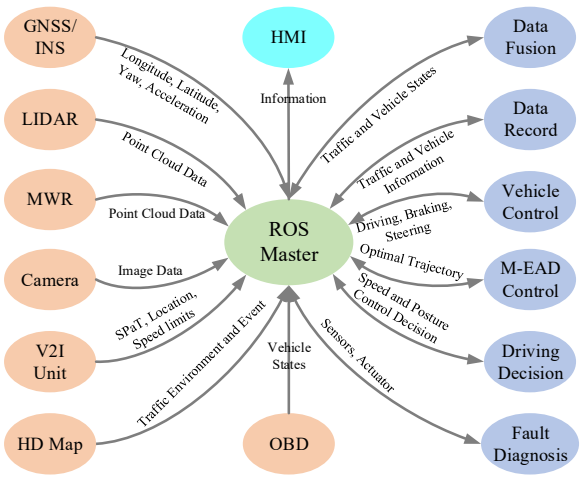

Fig. 21. Software node in ROS.

7.2 Experiment Results

Since we cannot obtain the instantaneous battery energy consumption of the test vehicle, only the SOC value was recorded. To make a fair comparison between different strategies, the changes in the SOC and vehicle kinetic energy are combined to evaluate the energy efficiency of the different strategies, as shown in Eq. (39).

$$E_v = 3600V_{oc}Q_b\left(SOC(0) - SOC(T_p)\right) - 0.5m\left(v^2(T_p) - v^2(0)\right) \tag{39}$$

where E_v is the approximated vehicle energy consumption.

Figs. 20-22 show the speed, distance, and battery power profiles obtained from the experiment, respectively. Note that the ideal trajectory is derived using I- and M-EAD strategies, and the real trajectory is the real movement of the test vehicle in both scenarios. Table 8 lists the results of SOC, energy consumption, and travel time obtained by all methods.

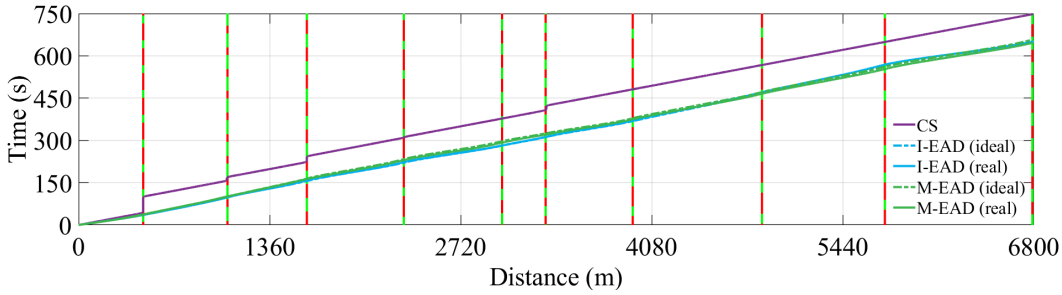

Fig. 20. Vehicle distance profile in the experiment.

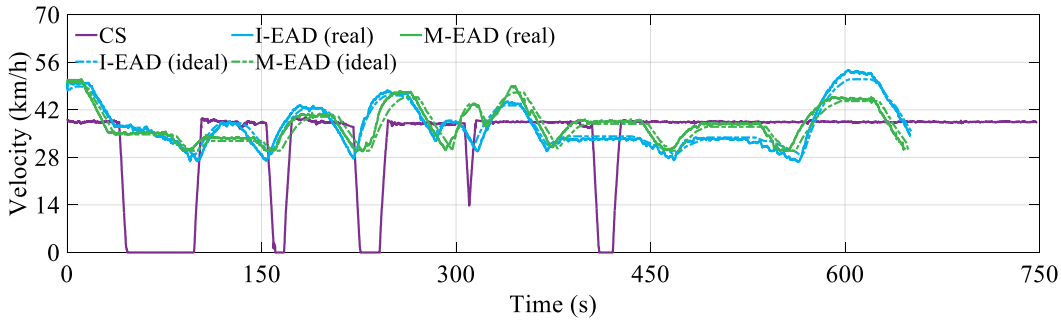

Fig. 21. Vehicle velocity profile in the experiment.

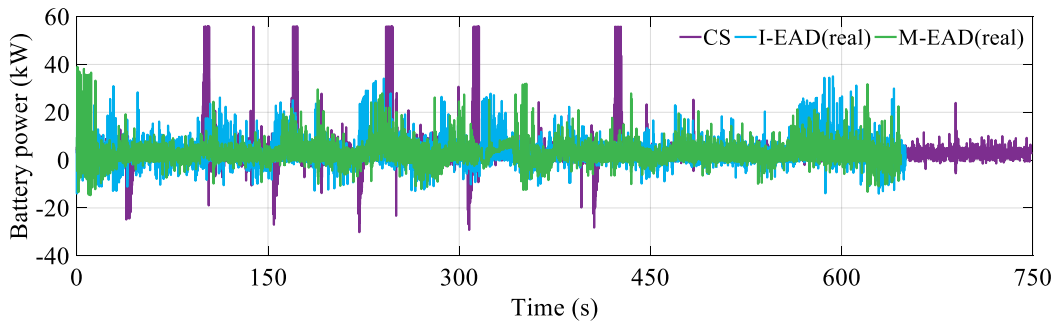

Fig. 22. Battery power profile in the experiment.

Table 8

Experiment results comparison for CS, I-EAD, and M-EAD strategies.

Strategy	State of charge		Approximated energy consumption		Travel time	
	Initial value (%)	Final value (%)	Value (kJ)	Improvement	Value (s)	Reduction (%)
CS	75.36	71.98	2399.10	4.66 (I-EAD vs. CS)	748.12	13.01 (I-EAD vs. CS)
I-EAD (real)	83.67	80.41	2287.25	15.00 (M-EAD vs. CS)	650.78	13.57 (M-EAD vs. CS)
M-EAD (real)	81.31	78.40	2039.28	10.84 (M-EAD vs. I-EAD)	646.61	0.64 (M-EAD vs. I-EAD)

As observed in Fig. 20, the vehicle with the M-EAD and I-EAD strategies drove the vehicle through all intersections without stopping, while the vehicle with CS strategy ended up with several stop-and-go operations. Compared to the CS, the battery energy consumption and travel time are reduced by 15.00 % and 13.57 % when M-EAD is applied, and 4.66% and 13.01 % of the I-EAD (see Table 8). This is because that the M-EAD and I-EAD can drive more smoothly compared to the CS by taking the intersection position and SPaT information into account so that inefficient acceleration and deceleration operations are reduced, so does the battery energy consumption (see Fig. 22). In addition, by reducing stop-and-go operations, M-EAD and I-EAD strategies result in shorter travel times. The M-EAD further improves energy efficiency by 10.84 % compared with I-EAD without incurring additional travel time. The main reason is that M-EAD takes all traffic signals positions and SPaT information along the path into account, which enables a more energy-efficient driving profile throughout the mission (see Figs. 21 and 22).

In terms of the tracking performance, the ideal and real speed profiles shown in Fig. 21 are compared. As it can be seen, the smooth optimal speed profile can be accurately tracked with the maximum speed tracking error of 3.98 % and 4.77 % for M-EAD and I-EAD strategies, respectively.

8. Conclusion

This paper proposes an eco-approach and departure strategy, namely M-EAD, which can enable a connected vehicle to drive through multiple signalized intersections with consideration of four key aspects during driving, energy consumption, travel time, and battery capacity loss, and driving comfort. A two-stage control scheme is proposed to coordinate efficient green signal window planning and vehicle speed optimization over the entire route. In the upper stage, the traffic signal green window is planned by formulating the shortest path problem which is solved with the A* algorithm; in the lower stage, the RHVO framework is designed to optimize the speed trajectory, where the energy efficiency, mobility, and battery life are optimized simultaneously by using the IDP algorithm. The M-EAD was validated evaluated using both offline Monte Carlo simulation tests and vehicle-on-road experiments carried out in an urban area of Nanjing.

The findings in this paper provide a new perspective on urban network eco-driving control in the context of connected EVs. More specifically, we first conduct a Monte Carlo simulation with randomized traffic light initial states. The comparative results against the CS strategy indicate that the proposed M-EAD strategy can noticeably improve the performance of the traditional control strategies. In contrast with the CS approach, the energy efficiency improvement and travel time saving of M-EAD can be up to 19.98 % and 35.95 %. The results also show that the average energy efficiency improvement and travel time saving of the M-EAD are respectively 6.55 % and 14.79 % when compared with the I-EAD strategy. Our results suggest that it is extremely beneficial to consider the SPaT information of the multiple intersections when designing an EAD strategy. Second, the proposed M-EAD strategy considers battery life. The simulation results demonstrate that with the aforementioned improvements in terms of energy efficiency and travel time, battery life can be prolonged by 10.51 % and 5.01 % on average utilizing M-EAD as compared to CS and I-EAD strategies, respectively. Since the longer battery life is a crucial performance index for EVs, it is necessary to consider battery health in the eco-driving strategy for EVs. Third, ride comfort is usually compromised when maximizing energy and travel time saving. The results shown in this paper demonstrate that the various savings led by the M-EAD in terms of energy, travel time, and battery life cost are achieved without sacrificing ride comfort. The experimental validation further confirms the benefits of M-EAD as compared to the traditional I-EAD and CS strategies.

In future, we will attempt to address more dynamic traffic conditions, including actuated traffic signal, nonstationary preceding traffic, by integrating intersection pass through probability prediction and optimal lane selection algorithm into the multiple intersections EAD control framework.

Acknowledgments

This work was supported by National Natural Science Funds for Distinguished Young Scholar under Grants 52025121, National Nature Science Foundation of China under Grants 52172383, 51975118, and 51805081.

References

[1] Stoicescu, A. P., 1995. On fuel–optimal velocity control of a motor vehicle. International Journal of Vehicle Design, 16(2-3), 229-256.

[2] Boriboonsomsin, K., Barth, M. J., Zhu, W., and Vu, A., 2012. Eco-routing navigation system based on multisource historical and real-time traffic information. IEEE Transactions on Intelligent Transportation Systems. 13(4), 1694-1704.

[3] Wang, M., Daamen, W., Hoogendoorn, S., and Van Arem, B., 2014. Potential impacts of ecological adaptive cruise control systems on traffic and environment. IET Intelligent Transport Systems. 8(2), 77-86.

[4] J. N, Barkenbus., 2010. Eco-driving: an overlooked climate change initiative. Energy Policy. 38(2), 762–769.

[5] Mensing, F., Bideaux, E., Trigui R., Ribet, J., and Jeanneret, B., 2014. Eco-driving: an economic or ecologic driving style? Transportation Research Part C: Emerging Technologies. 38, 110-121.

[6] Dib, W., Chasse, A., Moulin, P., Sciarretta, A., and Corde, G., 2014. Optimal energy management for an electric vehicle in eco-driving applications. Control Engineering Practice. 29, 299-307.

[7] U.S. Department of Energy, 2020. Next generation energy technologies for connected and automated on-road vehicles - 2020 annual program review. https://arpa-e.energy.gov/sites/default/files/0_NEXTCAR_AR_2020_final.pdf.

[8] Vahidi, A., and Sciarretta, A., 2018. Energy saving potentials of connected and automated vehicles. Transportation Research Part C: Emerging Technologies. 95, 822-843.

[9] Wang, Z., Bian, Y., Shladover, S. E., Wu, G., Li, S. E., and Barth, M. J., 2019. A survey on cooperative longitudinal motion control of multiple connected and automated vehicles. IEEE Intelligent Transportation Systems Magazine. 12(1), 4-24.

[10] Montanaro, U., Dixit, S., Fallah, S., Dianati, M., Stevens, A., Oxtoby, D., and Mouzakitis, A., 2019. Towards connected autonomous driving: review of use-cases. Vehicle System Dynamics. 57(6), 779-814.

[11] Zhuang, W., Qu, L., Xu, S., Li, B., Chen, N., and Yin, G., 2020. Integrated energy-oriented cruising control of electric vehicle on highway with varying slopes considering battery aging. Science China Technological Sciences. 63(1), 155-165.

[12] Ding, F., and Jin, H., 2018. On the optimal speed profile for eco-driving on curved roads. IEEE Transactions on Intelligent Transportation Systems. 19(12), 4000-4010.

[13] Wan, N., Vahidi, A., and Luckow A., 2016. Optimal speed advisory for connected vehicles in arterial roads and the impact on mixed traffic. Transportation Research Part C: Emerging Technologies. 2016, 69: 548-563.

[14] Xia, H., 2014. Eco-approach and departure techniques for connected vehicles at signalized traffic intersections. University of California, Riverside.

[15] Katsaros, K., Kernchen, R., Dianati, M., Rieck, D., and Zinoviou, C., 2011. Application of vehicular communications for improving the efficiency of traffic in urban areas. Wireless Communications and Mobile Computing. 11(12), 1657–1667.

[16] Li, S. E., Xu, S., Huang, X., Cheng, B., and Peng, H., 2015. Eco-departure of connected vehicles with V2X communication at signalized intersections. IEEE Transactions on Vehicular Technology. 64(12), 5439-5449.

[17] Ye, F., Hao, P., Qi, X., Wu, G., Boriboonsomsin, K., and Barth, M. J., 2018. Prediction-based eco-approach and departure at signalized intersections with speed forecasting on preceding vehicles. IEEE Transactions on Intelligent Transportation Systems. 20(4), 1378-1389.

[18] Dong, H., Zhuang, W., Chen, B., Yin, G., and Wang, Y., 2021. Enhanced eco-approach control of connected electric vehicles at signalized intersection with queue discharge prediction. IEEE Transactions on Vehicular Technology. 70(6), 5457-5469.

[19] Zeng, X., and Wang, J., 2018. Globally energy-optimal speed planning for road vehicles on a given route. Transportation Research Part C: Emerging Technologies. 93, 148-160.

[20] Shao, Y., and Sun, Z., 2020. Eco-approach with traffic prediction and experimental validation for connected and autonomous vehicles. IEEE Transactions on Intelligent Transportation Systems. 22(3): 1562-1572.

[21] Shao, Y., and Sun, Z., 2021. Energy-efficient connected and automated vehicles: real-time traffic prediction-enabled co-optimization of vehicle motion and powertrain operation. IEEE Vehicular Technology Magazine, 16(3), 47-56.

[22] Hao, P., Wu, G., Boriboonsomsin, K., and Barth, M. J., 2018. Eco-approach and departure (EAD) application for actuated signals in real-world traffic. IEEE Transactions on Intelligent Transportation Systems. 20(1), 30-40.

[23] Sun, C., Guanetti, J., Borrelli, F., and Moura, S. J., 2020. Optimal eco-driving control of connected and autonomous vehicles through signalized intersections. IEEE Internet of Things Journal. 7(5), 3759-3773.

[24] Ma, F., Yang, Y., Wang, J., Li, X., Wu, G., Zhao, Y., and Guvenc, L., 2021. Eco-driving-based cooperative adaptive cruise control of connected vehicles platoon at signalized intersections. Transportation Research Part D: Transport and Environment 92, 102746.

[25] Guo, Q., Angah, O., Liu, Z., and Ban, X. J., 2021. Hybrid deep reinforcement learning based eco-driving for low-level connected and automated vehicles along signalized corridors. Transportation Research Part C: Emerging Technologies. 124, 102980.

[26] Wegener, M., Koch, L., Eisenbarth, M., and Andert, J., 2021. Automated eco-driving in urban scenarios using deep reinforcement learning. Transportation Research Part C: Emerging Technologies. 126, 102967.

[27] Du, Z., HomChaudhuri, B., and Pisu, P., 2018. Hierarchical distributed coordination strategy of connected and automated vehicles at multiple intersections. Journal of Intelligent Transportation Systems. 22(2), 144-158.

[28] Chalaki, B., and Malikopoulos, A. A., 2021. Optimal control of connected and automated vehicles at multiple adjacent intersections. IEEE Transactions on Control Systems Technology. Doi: 10.1109/TCST.2021.3082306.

[29] B. Asadi., and A. Vahidi., 2010. Predictive cruise control: utilizing upcoming traffic signal information for improving fuel economy and reducing trip time IEEE Transactions on Control Systems Technology. 19(3), 707–714.

[30] Dong, S., Chen, H., Gao, B., Guo, L., and Liu, Q., 2021. Hierarchical energy-efficient control for CAVs at multiple signalized intersections considering queue effects. IEEE Transactions on Intelligent Transportation Systems.

[31] Yang, H., Almutairi, F., and Rakha, H., 2020. Eco-driving at signalized intersections: a multiple signal optimization approach. IEEE Transactions on Intelligent Transportation Systems. 22(5), 2943-2955.

[32] Lin, Q., Li, S. E., Du, X., Zhang, X., Peng, H., Luo, Y., and Li, K., 2018. Minimize the fuel consumption of connected vehicles between two red-signalized intersections in urban traffic. IEEE Transactions on Vehicular Technology. 67(10), 9060-9072.

[33] Lin, Q., Li, S. E., Xu, S., Du, X., Yang, D., and Li, K., 2020. Eco-driving operation of connected vehicle with V2I communication among multiple signalized intersections. IEEE Intelligent Transportation Systems Magazine. 13(1), 107-119.

[34] Wu, G., Hao, P., Wang, Z., and Jiang, Y., 2021. Eco-approach and departure along signalized corridors considering powertrain characteristics. SAE Int. J. Sust. Trans., Energy, Env., & Policy. 2(1), 1-16.

[35] Kumar, C. N., and Subramanian, S. C., 2016. Cooperative control of regenerative braking and friction braking for a hybrid electric vehicle. Proceedings of the Institution of Mechanical Engineers, Part D: Journal of Automobile Engineering. 230(1), 103-116.

[36] Johnson, V. H., 2002. Battery performance models in ADVISOR. Journal of Power Sources 110(2), 321-329.

[37] Wang, J., Liu, P., Hicks-Garner, J., Sherman, E., Soukiazian, S., Verbrugge, M., and Finamore, P., 2011. Cycle-life model for graphite-LiFePO4 cells. Journal of Power Sources. 196(8), 3942-3948.

[38] Li, S. E., and Peng, H., 2012. Strategies to minimize the fuel consumption of passenger cars during car-following scenarios. Proceedings of the Institution of Mechanical Engineers, Part D: Journal of Automobile Engineering. 226(3), 419-429.

[39] Hart, P. E.; Nilsson, N. J.; Raphael, B., 1968. A formal basis for the heuristic determination of minimum cost paths. IEEE Transactions on Systems Science and Cybernetics. 4(2): 100–107.

[40] Zhu, C., Lu, F., Zhang, H., Sun, J., and Mi, C. C., 2018. A real-time battery thermal management strategy for connected and automated hybrid electric vehicles (CAHEVs) based on iterative dynamic programming. IEEE Transactions on Vehicular Technology. 67(9), 8077-8084.

[41] Bellman, R. E., and Dreyfus, S. E., 2015. Applied dynamic programming. Princeton, NJ, USA: Princeton Univ. Press.